Bull Volcanol (2007) 69:609–626
DOI 10.1007/s00445-006-0098-x

RESEARCH ARTICLE

Volcanoes of the Tibesti massif (Chad, northern Africa)

Jason L. Permenter · Clive Oppenheimer

Received: 22 January 2004 / Accepted: 13 September 2006 / Published online: 24 November 2006

Abstract The Tibesti massif, one of the most prominent features of the Sahara desert, covers an area of some 100,000 km^2. Though largely absent from scientific inquiry for several decades, it is one of the world's major volcanic provinces, and a key example of continental hot spot volcanism. The intense activity of the TVP began as early as the Oligocene, though the major products that mark its surface date from Lower Miocene to Quaternary (Furon (Geology of Africa. Oliver & Boyd, Edinburgh (trans 1963, orig French 1960), pp 1–377, 1963)); Gourgaud and Vincent (J Volcanol Geotherm Res 129:261–290, 2004). We present here a new and consistent analysis of each of the main components of the Tibesti Volcanic Province (TVP), based on examination of multispectral imagery and digital elevation data acquired from the Advanced Spaceborne Thermal Emission and Reflection Radiometer (ASTER). Our synthesis of these individual surveys shows that the TVP is made up of several shield volcanoes (up to 80 km diameter) with large-scale calderas, extensive lava plateaux and flow fields, widespread tephra deposits, and a highly varied structural relief. We compare morphometric characteristics of the major TVP structures with other hot spot volcanoes (the Hawaiian Islands, the Galápagos Islands, the Canary and Cape Verdes archipelagos, Jebel Marra (western Sudan), and Martian volcanoes), and consider the implications of differing tectonic setting (continental versus oceanic), the thickness and velocity of the lithosphere, the relative sizes of main volcanic features (e.g. summit calderas, steep slopes at summit regions), and the extent and diversity of volcanic features. These comparisons reveal morphologic similarities between volcanism in the Tibesti, the Galápagos, and Western Sudan but also some distinct features of the TVP. Additionally, we find that a relatively haphazard spatial development of the TVP has occurred, with volcanism initially appearing in the Central TVP and subsequently migrating to both the Eastern and Western TVP regions.

Keywords Tibesti volcanic province · Tibesti massif · TVP · ASTER · Continental hot spot · Chad · African geology

Editorial responsibility: C. Kilburn

Electronic supplementary material Supplementary material is available in the online version of this article at http://dx.doi.org/10.1007/s00445-006-0098-x and is accessible for authorized users.

J. L. Permenter · C. Oppenheimer
Department of Geography, University of Cambridge,
Downing Place,
Cambridge CB2 3EN, UK

J. L. Permenter (✉)
Department of Geology and Environmental Geosciences,
College of Charleston,
66 George Street,
Charleston, SC 29424, USA
e-mail: volcano@jasonpermenter.com

Introduction

Located in the remote reaches of northern Chad, Africa, the Tibesti massif (Fig. 1a, b) has long been neglected by researchers due to the region's relative inaccessibility and history of political instability. Though largely absent from scientific inquiry for several decades, it is arguably one of the world's most significant examples of intracontinental volcanism. As much of our understanding of mantle hot spots has been obtained from observations of active volcanoes located in oceanic settings, the Tibesti massif and its related hot spot volcanics afford a valuable opportunity to explore the dynamics and properties of continental hot spot volcanism.

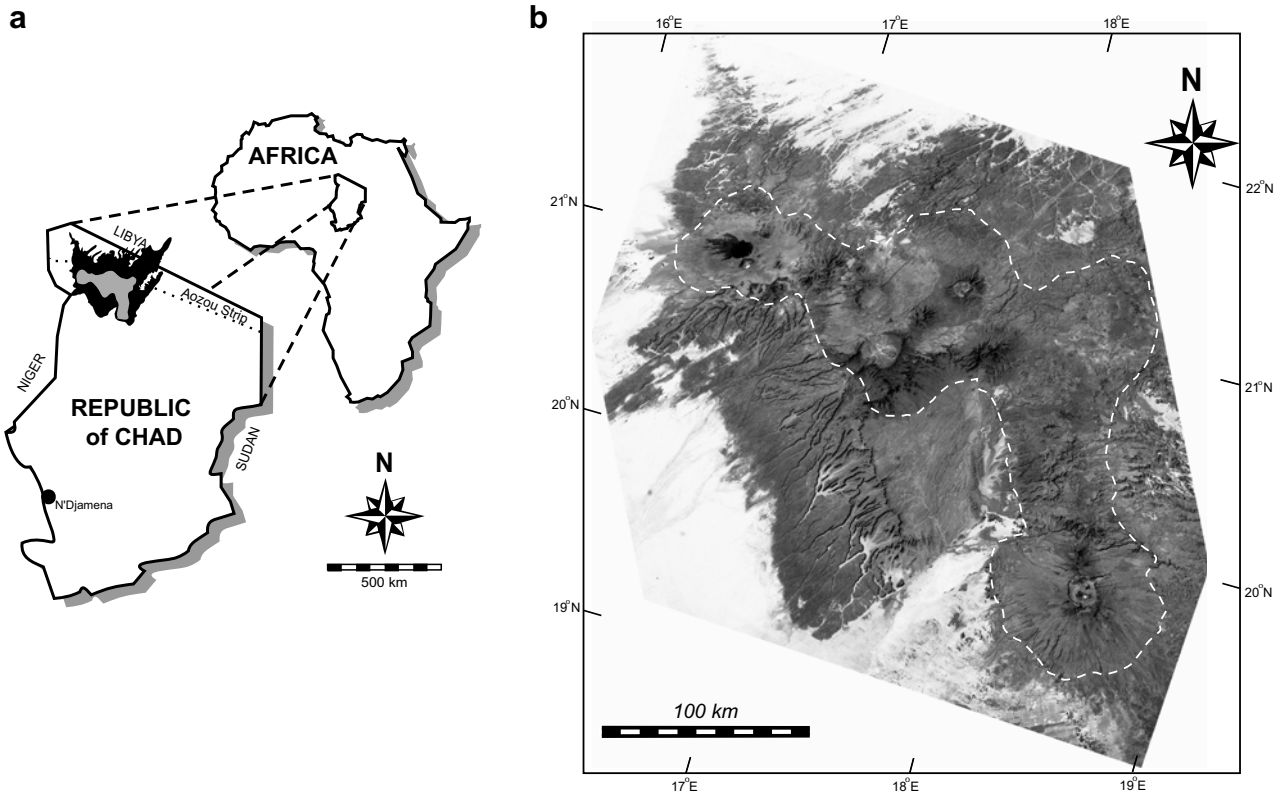

Fig. 1 **a** Location of the Tibesti massif (*black*) and the Tibesti Volcanic Province (*grey*), Chad, northern Africa; **b** International Space Station oblique photo of the Tibesti massif (Photo ID: ISS002-E-7327; 11 June 2001). The TVP can be seen in the central to lower portions of the massif (*outlined with dashed line*). The oblique nature of the photograph is such that the surface area increases *to the lower right* (south) within the figure. The northwest portion of the massif lies outside the photograph frame. (Image courtesy Earth Sciences and Image Analysis, NASA-Johnson Space Center. 27 June 2003)

In the early 20th Century, the region that includes the Tibesti massif was a contentious territory among the colonial powers of Africa. Due in part to the prospect of significant uranium deposits (Goodell 1992), conflict intensified in 1973 between the independent countries of Libya and Chad. Only in recent years has this 20-year-old border dispute been resolved by international agreement (Cohen 1994). Travel to the region is nonetheless problematic; estimates indicate that perhaps tens of thousands of land mines (International Campaign to Ban Landmines 2001) were planted in the Borkou–Ennedi–Tibesti area of northern Chad, and subsequently abandoned, before fighting was brought to an end. Landmine reports pertaining to Chad (Survey Action Center 2002) indicate that the Tibesti region remains most heavily contaminated with both mines and unexploded ordinance.

The most scientifically fruitful expeditions to the Tibesti massif were conducted between 1920 and 1970 by several teams, notably Tilho (1920), Gèze et al. (1959), Grove (1960), and Vincent (1970). Soon after, however, contest for control of the region made further geological research nearly impossible. General sketches of the geology and petrology of the Tibesti were provided by Gèze et al. (1959) and Vincent (1970). Malin (1977) investigated satellite images of large-scale Martian volcanism as analogues for the volcanism within the Tibesti massif. Apart from the geochemical and petrological work conducted by Gourgaud and Vincent (2004) on Emi Koussi (southeast Tibesti massif), we are unaware of any research published since these early works.

Although ground-based access to the Tibesti massif remains challenging, advances in satellite remote sensing do provide a basis for a modern synoptic survey of the volcanology of the region. Our aim here, in particular, is to exploit the sophisticated sensing capabilities of the Advanced Spaceborne Thermal Emission and Reflection Radiometer (ASTER) launched in December 1999 as part of NASA's Earth Observing System (EOS). This instrument provides not only multispectral imagery spanning the visible and infrared electromagnetic bands (with multiple channels in the shortwave and thermal infrared regions of the spectrum) but also permits retrieval of precision digital elevation data via its stereo imaging capability. A satellite-based analysis such as this is greatly enhanced by the excellent preservation of geologic features due to the aridity of the region. We evaluate

aspects of the Tibesti massif in the broader context of global hot spot volcanism. This systematic survey is also intended to provide a coherent framework of the Tibesti volcanism for any future studies of the region, including reconnaissance-scale field research.

Much of the toponymy of the Tibesti massif is derived from the Arabic and Teda-daza languages, and is used throughout the region. The term ehi refers to peaks or rocky hills, emi to larger mountains or mountainous regions, and tarso to high plateaux or gently-sloping mountainsides. Standard catalogues of terrestrial volcanoes (e.g. Simkin and Siebert 1994) list very few of the most identifiable Tibesti structures (limited solely to Emi Koussi, Tarso Toussidé, and Tarso Voon). In some cases, more than one place name may be found in the existing literature for the same feature within the Tibesti (e.g. Gèze et al. 1959; Grove 1960; Vincent 1970); for the sake of clarity and consistency, we choose here to use the most unambiguous and recognisable names. Additionally, we use here the terms dome and plateaux to refer to general topographic relief, and intend no reference to genetic or structural constraints unless otherwise indicated.

Location and geological setting

The Tibesti massif (see Fig. 1b) extends from approximately 19 to 23° N latitude and 16 to 19° E longitude (area ~100,000 km^2), and rises up to a maximum elevation of 3,394 km above the Saharan desert. For reference, the East African Rift system is located 1,900 km to the east, and the Cameroon hot spot is 1,800 km to the southeast. Though the political borders of the region have shifted repeatedly in the past, all of the volcanic portions of the Tibesti massif are now located within northernmost Chad, in the Borkou–Ennedi–Tibesti province.

The Tibesti massif is one of six major exposures of Precambrian crystalline rocks found in northern Africa. It consists of a core of intrusive and metamorphic rocks surrounded by Palaeozoic and younger sedimentary sequences, all of which are partly capped by Tertiary volcanic rocks (Ghuma and Rogers 1978). The ages of the basement rocks are not well known, but were radiometrically dated by Vachette (1964) as between 500–600 Myr. The Tibesti is separated from other massifs to the east and west by deep basins of Palaeozoic and younger sedimentary cover. To the north, it is bounded by a northward-thickening wedge of Palaeozoic, Mesozoic, and Tertiary sedimentary rocks. Southward, the massif connects with the older Precambrian terranes of central Africa, which are overlain by thin, mostly post-Palaeozoic sequences (Ghuma and Rogers 1978). From previous field campaign observations, the TVP has been generally assumed to be comprised of basalts, basanites, dacites, and youthful tephra deposits and ignimbrite sheets.

The term ‘hot spot’, in reference to the Tibesti region, reflects the broad concept as described by Morgan (1972) and Crough (1978) as a region of intra-plate or anomalous ridge crest volcanism that is either persistent or accompanied by a broad topographic swell. These characteristics have been noted for various oceanic swells and linear tracks of oceanic volcanism as partial evidence of upwelling plumes. Hot spots are typically associated with long-lived active volcanism, and are characterized by the advection of high heat flux to the earth’s surface (Smith and Braile 1994). Mantle plumes are interpreted to begin as instabilities near one of two major physical boundaries within the mantle: the upper/lower mantle boundary (~670-km deep) and the core-mantle boundary (~2,900 km depth) (Perfit and Davidson 2000). Low-density material travels buoyantly from depth through the mantle, displacing denser aesthenosphere, and ultimately heating the base of the lithosphere. This process ostensibly results in regional topographic uplift, lithospheric thinning, and magmatism. The mantle plume hypothesis is now widely accepted to explain the presence of hot spot volcanoes, but direct evidence for actual plumes is relatively weak; recent studies (Zhao 2001, 2004) have better explored the issues of delimiting and characterising mantle plumes via seismic modelling, and the locations of presumed hot spots have been correlated with a rise in the gravitational potential of the region (Perfit and Davidson 2000). Models for the distribution of volcanism in the context of plumes diverge, however. For example, White and McKenzie (1995) envisaged penetration of the lithosphere by numerous individual mantle plumes, while Ebinger and Sleep (1998) proposed that sub-lithospheric channelling of magma from a single, giant plume can laterally feed geographically discrete volcanic provinces (e.g. the Afar plume). The nature of hot spot volcanism in northern Africa has been comparatively little studied with respect to many other hot spot provinces.

Regional faults striking NNE–SSW follow Precambrian trends throughout the entire Tibesti region (El Makhrouf 1988), but are generally obscured within the TVP by the volcanic products. Malin (1977) recognised these faults as well, and suggested that subsequent uplift of the regional basement along a NNW axis was followed by the overall tilting to the NNE. Furon (1963) suggested that the northeast–southwest volcanic alignments of the northern Tibesti massif are an extension of those of the Cameroon Trough to the southwest, on the western continental margin of Africa. Guiraud et al. (2000) provided evidence for a 6,000 km, northwest–southeast striking lineament in northern Africa, extending from the volcanism of the East African Rift system, through the Tibesti massif, to the

northwest coast of the African continent. The relationships between this lineament and the volcanism of the Tibesti, if any, have not yet been determined.

Centroid-Moment Tensor (CMT) solutions from the Harvard University Seismology group suggest that the Tibesti region has been effectively aseismic, at least above Mw ~5.5, since data have been recorded in northern Africa from 1976 (cf. Dziewonski et al. 1981).

Our preliminary inspection of the EGM96 spherical harmonic model of the Earth's gravitational potential indicates a significant positive gravity anomaly beneath the TVP, though wavelength limitations of current gravity model data for the region limit interpretations of sub-surface lithosphere–aesthenosphere interactions.

Remote sensing and data processing

Due to the aridity of the Sahara, the Tibesti massif is nearly free of accumulated vegetal soil, and robust plant life is deficient in almost every area throughout the year. Conditions highly favour exposure of the region's geological features, particularly when viewed using remote sensing data. The utility of remote sensing techniques in studying volcanic regions on Earth is well documented (e.g. de Silva and Francis 1990; Okada and Ishii 1993; Kahle et al. 1995; Oppenheimer 1998; Ramsey et al. 2004; Wiart and Oppenheimer 2005), and, of course, research on planetary volcanism has depended almost exclusively on remote sensing (e.g. Malin 1977; Mouginis-Mark and Robinson 1992; Davies et al. 2001). Both ground-based and spaceborne remote sensing data provide a unique perspective on large- and small-scale volcanic processes. With careful analysis and interpretation of spectral reflectance, image texture, and topographical data, rich palaeovolcanological, lithological and related information can be extracted.

Our primary source of remote sensing data used in this study is the multispectral Advanced Spaceborne Thermal Emission and Reflection Radiometer (ASTER; Table 1). ASTER is an imaging instrument carried on Terra, a satellite launched in December 1999 as part of NASA's Earth Observing System (EOS). The characteristics and capabilities of the ASTER instrument have been discussed elsewhere in detail (e.g. Kahle et al. 1991; Yamaguchi et al. 1998; Pieri and Abrams 2004), and are summarised here in Table 2. The multispectral data were digitally processed using the ENVI (v. 3.6 and 4.0) imaging software (Research Systems, Inc.) on a PC platform. Each ASTER scene containing volcanic features was treated using well-established image processing techniques, all designed to enhance the spectral, spatial, and textural characteristics of the imagery. In total, we have utilized 51 individual scenes (Table 3) to cover the entire volcanic portion of the Tibesti massif in Chad (one scene covers approximately 60×60 km).

Digital elevation models (DEMs) were produced for each of the volcanic features by making use of the stereo capabilities of the ASTER instrument. Separate sensors exist for ASTER band 3, each viewing the Earth's surface at different look-angles (nadir and aft) to allow stereoscopic analyses. Much of the description and analysis presented within this investigation was based on study of interactive perspective views of the Tibesti volcanism in various user-defined combinations of spectral channels (Fig. 2).

Table 1 Spectral wavelength resolution characteristics of ASTER

Subsystem	Band	Spectral range (μm)	Spatial resolution (m)
VNIR	1	0.52–0.60	15
	2	0.63–0.69	15
	3n, 3b[a]	0.76–0.86	15
SWIR	4	1.600–1.700	30
	5	2.145–2.185	30
	6	2.185–2.225	30
	7	2.235–2.285	30
	8	2.295–2.365	30
	9	2.360–2.430	30
TIR	10	8.125–8.475	90
	11	8.475–8.825	90
	12	8.925–9.275	90
	13	10.25–10.95	90
	14	10.95–11.65	90

ASTER instrument spectral wavelength resolution

[a] Band 3 is split into one nadir- and one backward-looking view for use in stereographic analysis.

Table 2 ASTER instrument capabilities

Performance capabilities	Values
Stereo base-to-height ratio	0.6 (band 3)
Swath width	60 km (all bands)
Total edge-to-edge coverage capability in cross-track direction	±136 km (all bands)
Cross-track pointing capability (array center)	±8.54° (all bands)
Signal quantization	8 bits (bands 1–9) 12 bits (bands 10–14)
Modulation transfer function (MTF) at Nyquist frequency	0.25 (all bands)
Peak data rate	89.2 Mbit/s (all bands including stereo)
Mission life	5 years
Mass	352 kg
Maximum power	650 W
Physical size	1.6×1.6×0.9 m^3

ASTER instrument performance capabilities (after Kahle et al. 1991)

Table 3 Selected ASTER satellite imagery covering the Tibesti Volcanic Province, northern Chad

Location	ASTER image filename	Image acquisition date, time (local)	Image centerpoint	
			Lat (°N)	Lon (°E)
Western Tibesti	pg-PR1B0000-2001121002_037_001	02 Oct 2000, 09:47:18	21.54	16.29
	pg-PR1B0000-2001121002_038_001	02 Oct 2000, 09:47:27	21.01	16.17
	AST_L1A_003_04212001093715_05042001085402	21 Apr 2001, 09:37:16	21.45	18.52
	pg-PR1B0000-2001052502_040_001	14 May 2001, 09:43:09	20.43	16.39
	pg-PR1B0000-2001052502_039_001	14 May 2001, 09:42:51	21.49	16.64
	AST_L1A_003_05212001094857_05302001162923	21 May 2001, 09:48:57	21.25	16.76
	pg-PR1B0000-2001111104_140_001	28 Oct 2001, 09:44:16	21.30	16.47
	pg-PR1B0000-2001111104_072_001	28 Oct 2001, 09:44:25	20.76	16.34
	pg-PR1B0000-2001121602_040_001	29 Nov 2001, 09:43:30	21.36	16.06
	pg-PR1B0000-2002051302_103_001	01 May 2002, 09:34:51	20.95	16.56
	pg-PR1B0000-2002051902_080_001	08 May 2002, 09:40:45	21.34	16.18
	pg-PR1A0000-2002070201_009_023	18 Jun 2002, 09:34:40	21.44	17.02
	pg-PR1A0000-2002101001_035_001	05 Aug 2002, 09:34:51	21.00	16.20
	pg-PR1B0000-2002101702_102_001	23 Sep 2002, 21:12:22	20.85	16.53
	pg-PR1B0000-2002101702_134_001	23 Sep 2002, 21:12:31	21.38	16.41
	AST_L1B_003_02132003093424_03112003191639	13 Feb 2003, 09:34:25	20.96	16.55
Western/Central	AST_L1A_003_11062001093756_11192001140442	06 Nov 2001, 09:37:56	20.91	16.88
	pg-PR1A0000-2002070201_009_024	18 Jun 2002, 09:34:49	20.91	16.90
Central Tibesti	AST_L1A_003_02072001094520_05312001112114	07 Feb 2001, 09:45:20	20.82	17.50
	pg-PR1B0000-2001081102_043_001	02 Aug 2001, 09:41:00	21.90	17.68
	pg-PR1B0000-2001081102_126_001	02 Aug 2001, 09:41:09	21.36	17.56
	pg-PR1B0000-2001081102_044_001	02 Aug 2001, 09:41:26	20.30	17.31
	pg-PR1B0000-2001112003_115_001	06 Nov 2001, 09:37:47	21.44	17.01
	pg-PR1B0000-2001112003_191_001	06 Nov 2001, 09:37:56	20.91	16.89
	pg-PR1B0000-2002020402_070_001	09 Jan 2002, 09:35:52	20.85	17.27
	pg-PR1B0000-2002021002_190_001	18 Jan 2002, 09:29:44	20.42	17.98
	AST_L1B_003_07042002093501_08062002161014	04 Jul 2002, 09:35:01	20.87	17.18
	pg-PR1B0000-2002080702_053_001	05 Jul 2002, 21:12:38	20.94	17.16
	AST_L1B_003_10082002093418_12082002084659	08 Oct 2002, 09:34:18	20.75	17.96
	AST_L1B_003_01062003210533_02032003095824	06 Jan 2003, 21:05:33	20.72	17.18
	AST_L1B_003_01122003093414_01282003131601	12 Jan 2003, 09:34:14	20.85	17.29
	AST_L1B_003_01122003093423_01282003122031	12 Jan 2003, 09:34:23	20.32	17.16
Central/Eastern	AST_L1A_003_08082000094140_10202002151844	08 Aug 2000, 09:41:41	21.00	17.79
	pg-PR1B0000-2002021002_135_001	18 Jan 2002, 09:29:35	20.95	18.10
	pg-PR1B0000-2002022002_220_001	03 Feb 2002, 09:29:18	20.96	18.06
	AST_L1A_003_02032002092918_02192002191937	03 Feb 2002, 09:29:19	20.96	18.07
	pg-PR1B0000-2002022002_179_001	03 Feb 2002, 09:29:27	20.43	17.94
	AST_L1A_003_12042002092836_12182002123907	04 Dec 2002, 09:28:37	20.96	18.04
Eastern Tibesti	pg-PR1B0000-2001070502_266_001	16 Jul 2000, 09:36:38	19.36	19.21
	AST_L1A_003_04212001093742_05042001085507	21 Apr 2001, 09:37:42	19.84	18.15
	AST_L1A_003_05232001093633_06012001160001	23 May 2001, 09:36:33	21.45	18.49
	AST_L1A_003_05232001093659_06012001160054	23 May 2001, 09:37:00	19.85	18.12
	pg-PR1B0000-2002012902_103_001	02 Jan 2002, 09:29:56	21.40	18.88
	pg-PR1B0000-2002012902_104_001	02 Jan 2002, 09:30:05	20.86	18.76
	pg-PR1B0000-2002012902_209_001	02 Jan 2002, 09:30:14	20.33	18.63
	pg-PR1B0000-2002012902_105_001	02 Jan 2002, 09:30:22	19.79	18.51
	AST_L1A_003_01022002093022_01282002183414	02 Jan 2002, 09:30:23	19.79	18.51
	pg-PR1B0000-2002021002_233_001	18 Jan 2002, 09:29:26	21.49	18.23
	pg-PR1B0000-2002022002_219_001	03 Feb 2002, 09:29:09	21.49	18.19
	AST_L1A_003_11182002092825_12012002130008	18 Nov 2002, 09:28:25	19.78	18.58
	AST_L1B_003_12292002092226_01172003120744	29 Dec 2002, 09:22:26	19.93	19.06

The filename structure is a convention of the ASTER Data Acquisition Team (NASA/Japan)

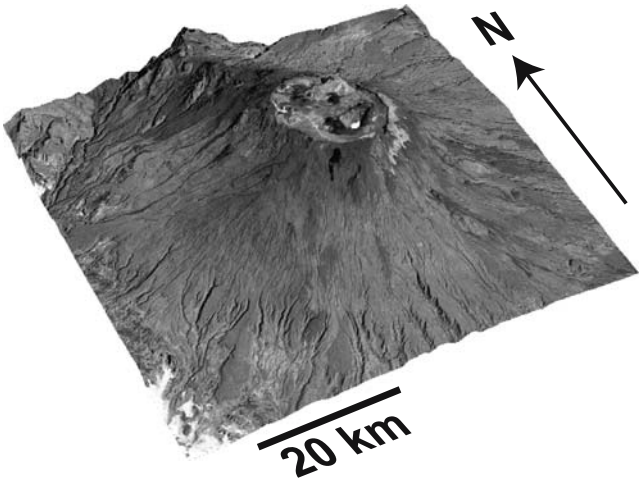

Fig. 2 Digital elevation model (DEM) of the Emi Koussi volcano (q.v.), eastern Tibesti, with the corresponding ASTER bands 3, 2, and 1 (as R, G, B) draped on top (total relief=2,894 m; vertical exaggeration=4×). The DEM was created using the nadir- and backward-looking capabilities of the ASTER imaging system for stereoscopic viewing. In plan view, the dimensions of this scene are approximately 60×60 km. Image ID pg-PR1B0000-2002012902_105_001; bands 3,2,1 as R,G,B

In addition to its high spatial resolution, the ASTER instrument was deliberately designed for enhanced spectral resolution in the short-wave and thermal infrared channels (SWIR and TIR, respectively) with geologists in mind; these additional spectral bands facilitate better discrimination of mineralogy and lithology in satellite imagery. The wide range of wavelengths covered by ASTER (see Table 1) allows good quality distinction between iron oxide minerals, clay-bearing minerals, sulphate minerals, ammonia minerals, siliceous rocks, and carbonates (e.g. Kahle and Goetz 1983). Other researchers (e.g. Abrams and Hook 1995; Hubbard et al. 2003) have used simulated ASTER data to produce geologic maps of unaltered and hydrothermally altered volcanic areas that are as accurate as published maps made by traditional field methods.

In this study, we have relied solely upon the use of several combinations of ASTER spectral channels to help resolve basic lithologies of the TVP (translated to R G, B for image processing). Fundamental distinctions between tephra deposits, basalts, and sandstone regions of the Tibesti region were made possible by the use of decorrelation contrast stretches within the TIR wavelengths of the ASTER imagery, and were compared on a first-order basis to existing, yet limited, studies of the Tibesti lithology (e.g., Vincent 1970; Gourgaud and Vincent 2004) as ad hoc field data. Stretching the spectral data by this process produces spectral differences between surface units to be displayed as colour differences in R, G, B, while most of the temperature variation prevalent in thermal wavelengths is displayed as differences in intensity. We recognize that limitations abound in detailing the Tibesti volcanic lithologies, however, due to an obvious paucity of ground-based sampling or comparison. For this reason, we do not present extensive lithologic mapping of the Tibesti massif within this particular study.

Important supplementary databases used were Landsat Thematic Mapper (TM) images, and 70-mm astronaut photography from the Space Shuttle (STS087-717-075, 19 November–5 December 1997; STS102-717-60, 19 March 2001; STS108-701-008, 5–17 December 2001; Earth Sciences and Image Analysis 2003). The latter provides natural colour images at variable illuminations and look angles with a nominal ground resolution of ~20 m under optimal circumstances.

Volcanoes of the Tibesti massif

Though the areal extent of the Tibesti massif is some 100,000 km^2, most of the volcanism is confined to a region in the southern section, which we here refer to as the Tibesti Volcanic Province (TVP), covering approximately one-third of the massif's total area. Loosely defined geographical boundaries within the TVP provide a basis for dividing the TVP into three sub-provinces: the Eastern, Central, and Western regions; this classification does not suggest genetic or structural significance, and is used within this study for sake of ease. Detailed and extensive descriptions of the primary TVP volcanic structures, including three-dimensional animations, can be found online as Electronic supplementary material. A summary of the characteristics of the volcanoes and associated features of the Tibesti can be found in Table 4. For the general location map of the main volcanic centres and other features, refer to Fig. 3.

Evolution of the Tibesti volcanic province

Concrete evidence of the chronology of Tibestian eruptive activity is very sparse, though Quaternary volcanic ash deposits were emplaced into standing bodies of water (e.g. Trou au Natron) where diatoms flourished (Furon 1963). Field samples from the Tibesti with any useful locality information have proved equally difficult to acquire. At present, the most productive means for determining the volcanic history of the Tibesti lies with interpretation of the satellite imagery. Due to the areal extent of the TVP, age relations amongst the volcanoes are difficult to discern; in the absence of quantitative fieldwork, however, remote sensing imagery does shed some light on the sequence of events. Given the nature of the available data, we stress that the age relationships described for the volcanic features are based

Table 4 Characteristics of the prominent volcanic features within the Tibesti Volcanic Province, northern Chad

	Feature	Latitude (°N)	Longitude (°E)	Feature type	Maximum elevation (m)	Edifice height (m)	Area (km^2)	Width (km)	Caldera dimensions (km)	Caldera depth (m)	Crater width (km)	Crater depth (m)
Eastern TVP	Emi Koussi	19.86	18.54	Sd	3,394	770	2,945	60×80	9.0×12	300, 450	–	–
	Era Kohor	19.53	18.56	C	–	–	4.14	–	–	–	2.5–3.0	330
	Tarso Ahon	20.38	18.30	VP	2,780	1,120	~3,000?	50×60	–	–	–	–
	Tarso Emi Chi	21.43	18.40	VP	2,690	1,060	7,700	70×110	–	–	–	–
	Tarso Aozi	21.18	18.57	VP	2,530	–	6,500	100×65	–	–	–	–
	Tarso Mohi	20.70	18.22	VP	2,274	–	1,200	40×30	–	–	–	–
Central TVP	Tarso Ourari	21.32	17.53	VP	~1,450	~1,100	~700	50×16	–	–	–	–
	Tarso Tieroko	20.77	17.87	CD	2,925	~1,350	~570	33×30	7.0×9.7	~775	–	–
	Bounaï	20.87	17.97	D	2,169	1,866	3.6	2.2×2.2	–	–	–	–
	Tarso Toon	21.07	17.62	Sd	2,575	~1,600	600	19×21	11×12	494	–	–
	Ehi Yéy	20.85	17.53	CD	2,774	~ 1,950	200	16×13	11×7.5	524	–	–
	Tarso Voon	20.92	17.27	Sd	2,845	2,200	~1,700	40×60	12×13	~ 1,000	–	–
	Ehi Sunni	20.81	17.4	D	2,820	~2,400	4.5	3.8×3.3	–	–	–	–
	Tarso Yega	20.66	17.42	Sd	2,972	~1,500	960	26×33	19×20	~ 300	–	–
	Ehi Mousgou	21.06	17.14	CD	2,849	~2,000	32.41	5.7×5.0	–	–	–	–
	Soborom	20.99?	17.18?	TD	~2,800	~2,250	36.20?	9.9×8.2?	–	–	–	–
	Tarso Abeki	21.00	16.99	CD	2,691	1,500	446.8	29×20	13×10	491	–	–
Western TVP	Ehi Sosso	21.00	16.72	D	2,657	2,280?	18	5.1 diam	–	–	–	–
	Doon Kidimi	21.03	16.61	C	2,580	–	1.95	–	–	–	1.3×1.7	364
	Tarso Tamertiou	20.88	16.80	VP	2,724	~1,900	98	7.2×9.0	–	–	–	–
	Timi	21.16	16.58	D	3,012	2,200	15	4.7×4.1	–	–	–	–
	Tarso Toussidé	21.04	16.47	Sd	~2,600	~900	~1,900	46×52	–	–	–	–
	pre-Toussidé calderas	21.03	16.59	Cal	2,482	~2,550	~150 (32 visible)	–	16×13; 9.5 diam	>267	–	–
	Trou au Natron	20.98	16.57	C	2,425	–	40	–	–	–	8.01 diam	768
	Pic Toussidé	21.04	16.47	S	3,296	2,230	44	8.1 diam	–	–	–	–
	Tôh	21.34	16.43	VP	2,065	1,150	490	43×23	–	–	–	–

Dimensions of features that have proved spurious or impossible to determine using remote sensing techniques have been qualified with a ?, indicating that such values should be viewed with some scepticism, and are in any case not intended to be authoritative. Elliptical and sub-elliptical edifices have dimensions for both the long- and short-axes reported, and irregularly-shaped features have associated ranges of measurements indicated.

C Crater, *Cal* caldera, *CD* complex dome, *D* isolated dome, *Com* composite volcano, *Sd* shield volcano, *TD*, thermal dome, *VP* volcanic plateau.

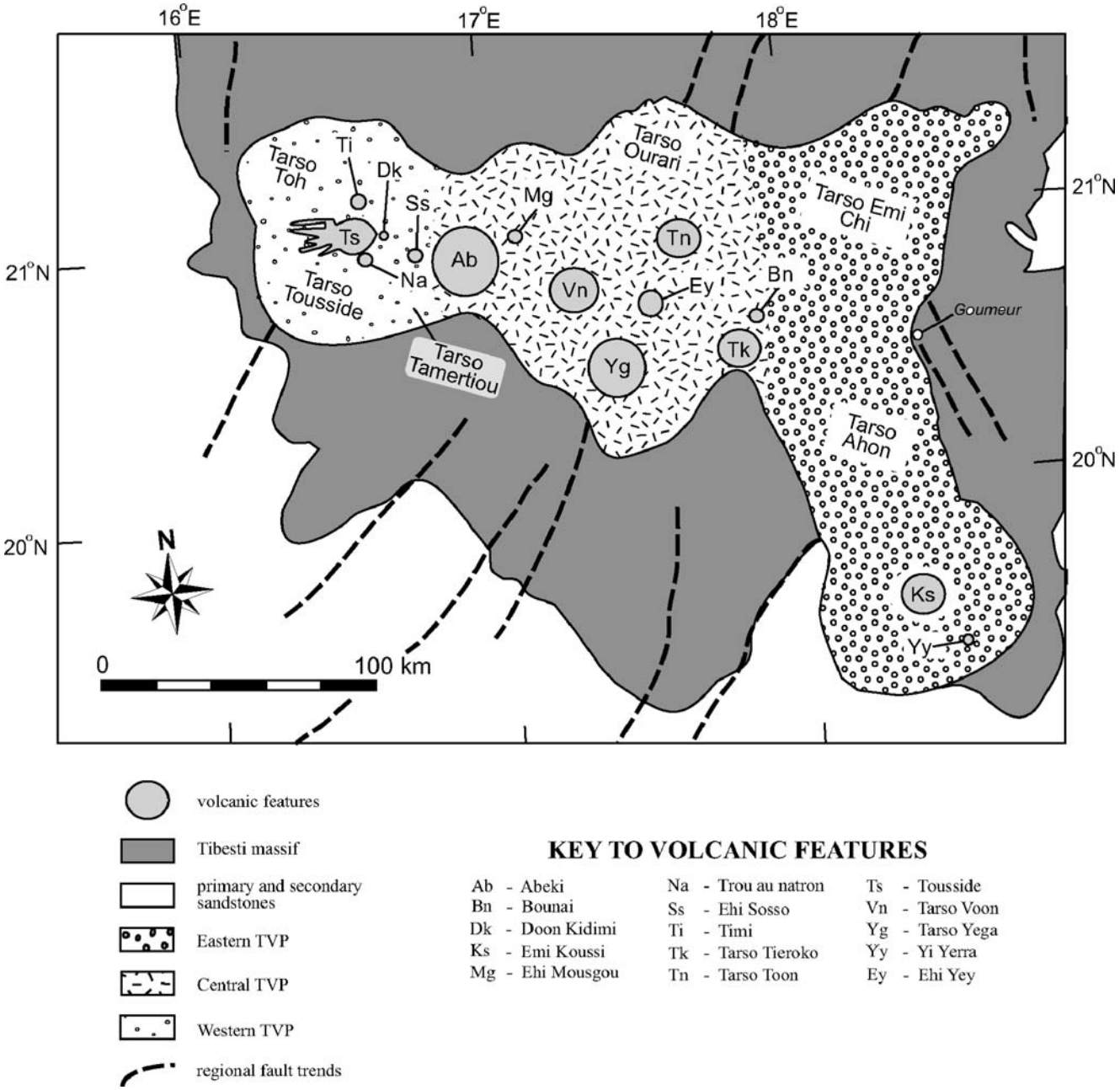

Fig. 3 Principal features and characteristics of the Tibesti Volcanic Province, Tibesti Massif, northern Chad

here on superposition and embayment relationships of the volcanic units currently exposed at the surface, which are assumed to be predominantly the youngest materials associated with each feature.

Some relative dating information and other basics have been established over many decades, however. The TVP volcanics directly overlie Precambrian basement granites, diorites, and crystalline schists (Gèze et al. 1959). The basement rock is, in turn, completely surrounded and overlapped by flat-lying sediments of the Sahara Desert (Cahen et al. 1984). The intense activity of the TVP began perhaps as early as the Oligocene, though the major products that mark its surface occurred during the Quaternary (Furon 1963; Gourgaud and Vincent 2004). As reference, we note that Gourgaud and Vincent (2004) suggest an age of Lower Miocene for the initial thrust of volcanic activity and lava effusion in the Tibesti Volcanic Province, with a somewhat younger estimate for the majority of Emi Koussi products of 2.42 to 1.32 Myr. Here, we present the succession of volcanism within the Tibesti, based primarily on interpretation of the satellite imagery (Fig. 4). We stress that these divisions (Phase 1, Phase 2, etc.) do not necessarily denote changes in volcanic styles or significant breaks in volcanic or tectonic activity, but represent convenient groupings of the observed volcanic history of the Tibesti volcanism. Additionally, we do not infer details of the subsurface magmatic

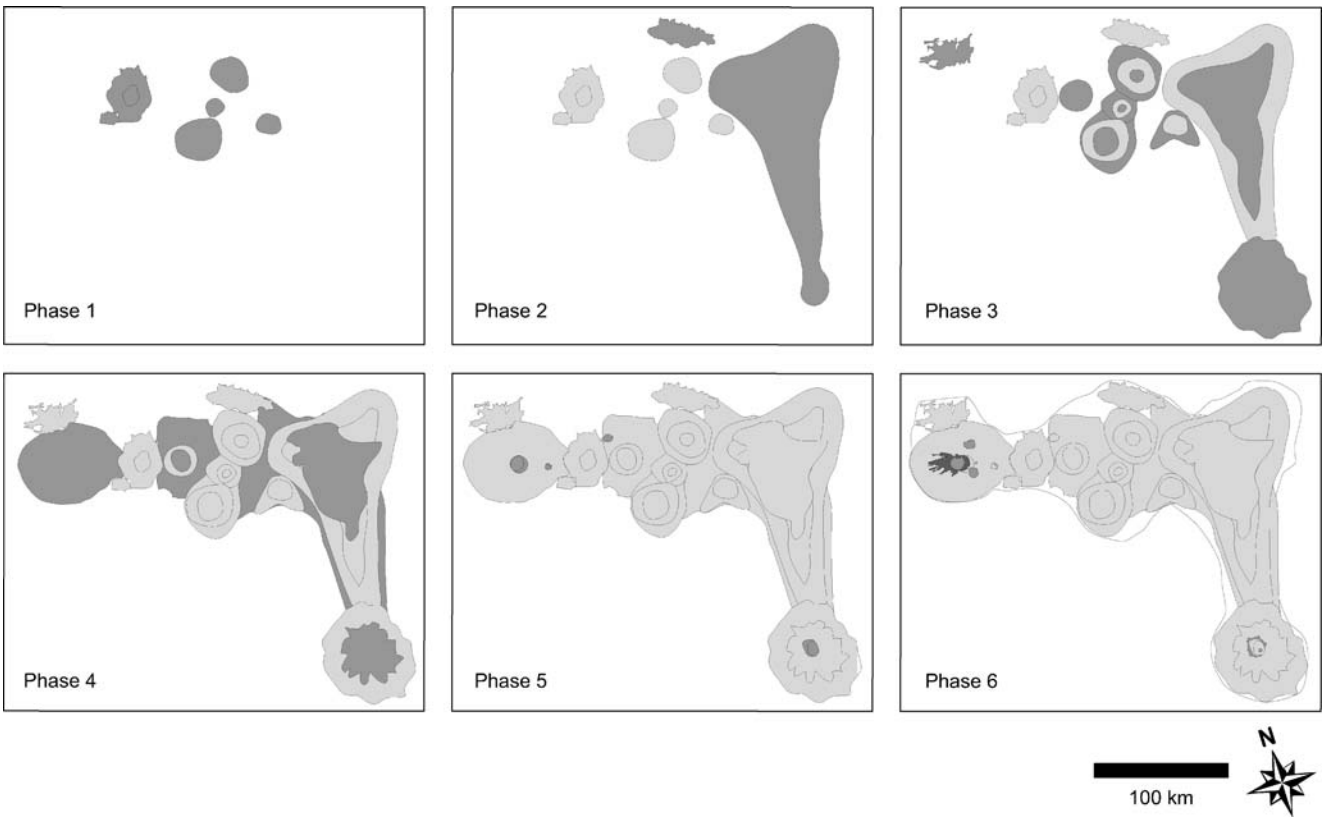

Fig. 4 Simplified interpretation of six evolutionary phases of volcanism within the TVP

plumbing system. A short description of the main features within each phase in the TVP volcanic evolution is summarized in Table 5.

Phase 1

The initial phase of volcanism began in the Central TVP, following an inferred uplift and extension of the Precambrian basement. The relative dating of these volcanic products is based on the close proximity of the structures and their reasonably distinct deposits. Based on the ostensibly high degree of weathering of its central and flank regions, we suggest that the development of Tarso Abeki and its lava flows began early in the TVP history. Formation and growth of Tarso Tamertiou, Tarso Tieroko, Tarso Yega, Tarso Toon, and Ehi Yéy followed. Any deposits from their early activity have been obscured by subsequent eruptions.

Phase 2

The second phase consists of activity spreading north and east from the Central TVP. This migration formed not only Tarso Ourari, but the initial lava emplacement of the Eastern TVP as well. Volcanism also spread to the southeast, with the formation of Emi Koussi.

Gèze et al. (1959) indicated ancient ignimbrite deposits hidden beneath many portions of the Eastern TVP (the source as yet undetermined), including Emi Koussi to the southeast. These deposits are difficult to distinguish in satellite imagery, but if present would suggest earlier activity in that region contemporaneous to, or just after, the full-scale volcanism of the Central TVP.

Phase 3

It is during this middle stage that the eruptions and deposition of extensive lavas and tephra deposits from Tarso Yega, Tarso Toon, Tarso Tieroko, and Ehi Yéy took place in the Central TVP. Associated with Tarsos Yega and Tieroko were the effusive eruptions of lavas; large-scale, explosive eruptions leaving tephra deposits; and subsidence of the summit regions and caldera formation. The lack of a well-defined topographic rim or caldera floor at Tieroko might suggest structural variations in the style of magma chamber tapping, or differences in magma composition and flux from that at Tarso Yega. Also seen were further caldera collapse and associated widespread tephra deposits from Tarso Yega, as well as the appearance of lavas that make up the darker-toned Ehi Yéy, Tarso Tieroko, and Bounaï structures.

Several stages of lava emplacement have occurred within the large plateaux regions of the Eastern TVP, and

Table 5 Phase evolution summary of the volcanism, structures, and products of the Tibesti Volcanic Province, northern Chad

	Western TVP	Central TVP	Eastern TVP
Phase 1		Uplift and extension of the Precambrian basement; appearance and growth of Tarso Abeki lava flows, followed by formation of Tarso Tamertiou, Tarso Tieroko, Tarso Yega, Tarso Toon, and Ehi Yéy	
Phase 2		Emplacement of Tarso Ourari to north	Large-scale ignimbrite deposits throughout[a]; initial phases of large-scale lava field emplacement; appearance of volcanism in the southeast to begin Emi Koussi volcanism
Phase 3		Effusive eruptions of lava, caldera formation, and tephra deposition associated with Tarso Yega and Tarso Tieroko; appearance of lavas of the Ehi Yéy, Tarso Tieroko, and Bounaï structures; full appearance of Tarso Voon	Continued lava emplacement (Tarso Emi Chi, Tarso Mohi, Tarso Ahon); continued construction of Emi Koussi volcano
Phase 4	Uplift and formation of Tarso Toussidé, lava effusion associated with Tarso Tôh	Caldera collapse at the summit of Tarso Voon and associated extensive tephra deposition	Continued lava emplacement throughout, though at a decreased rate; sustained build-up of lavas and tephra at Emi Koussi
Phase 5	Appearance of nested caldera system of Tarso Toussidé and associated tephra deposition; formation of Ehi Sosso	Extrusion of lavas at Ehi Mousgou	Lava production continues to wane; appearance of nested caldera system of Emi Koussi
Phase 6	Formation of Pic Toussidé and the appearance of its dark-toned lava flows; appearance of lava flows making the Timi structure; formation of Trou au Natron and Doon Kidimi		Lava flow and minor pyroclastic deposit emplacement on Emi Koussi flanks; appearance of minor cinder cones on flanks and within the summit calderas of Emi Koussi; formation of Era Kohor crater at Emi Koussi summit.

The divisions envisioned here (Phase 1, Phase 2, etc.) do not deliberately reflect changes in volcanic style or significant breaks in volcanic or tectonic activity, and are instead merely convenient groupings of the observed volcanic history of the Tibesti volcanism.
[a] Source unknown

individual phases are thought here to be distributed sporadically throughout the Tibesti Volcanic Province's timeline of activity; the emplacement of lava flows from numerous vents formed the large volcanic plateaux of Tarsos Emi Chi, Mohi, and Ahon. These regions have been somewhat subjectively delineated in previous literature, and have no obvious relationships to the surrounding volcanics, apart from their relative position within the Eastern TVP. Furthermore, this phase of the TVP volcanism included activity that continued the initial construction of the Emi Koussi composite volcano to the south.

Based on stratigraphic relationships, textures of its products, and characteristics of its caldera structure in satellite imagery, we suggest that the full appearance of Tarso Voon within the Central TVP took place during this phase.

Phase 4

Lava emplacement within the Eastern TVP continued, though, according to Gèze et al. (1959), at a lower rate. We suggest that during this phase the emplacement of lavas associated with the Eastern TVP activity continued filling the geographical boundary between the Eastern and Central provinces; as stated, however, the timing is uncertain. It is likely that the sustained build-up of lavas and tephra at Emi Koussi also characterises this phase, though solid evidence for the timing of Koussi's activity is difficult to discern due to its relative detachment from potential stratigraphic relationships within the rest of the TVP.

Within Phase 4, we also see the formation of Tarso Toussidé in the Western TVP. Contemporaneously, there was caldera collapse at the summit of Tarso Voon, and deposition of its associated extensive tephra took place, which mantled a large portion of the Central TVP.

Elsewhere, to the northwest of the Western TVP, the far-reaching lava flows associated with Tarso Tôh seem to be intermediate in both texture and weathering in satellite imagery, and are similar in those respects to the lava plateaux of the Eastern TVP, perhaps suggesting that the emplacement for at least a portion of these flows is broadly

contemporaneous. Sediments within the Begour maar of Tarso Tôh have been radiocarbon dated at 8,300±300 years (Hagedorn and Jakel 1969).

Phase 5

During Phase 5, lava production in the Eastern TVP wanes further still, and most of the large-scale activity throughout the TVP had abated. The most striking activity during this stage, however, was the development of the nested caldera systems of both Tarso Toussidé (Western TVP) and Emi Koussi (Eastern TVP). Compared to the extensive tephra deposits left by the collapse at Tarso Toussidé, Emi Koussi shows less evidence of widespread tephra deposition on its flanks, though the effects of aeolian erosion and perhaps precipitation should not be overlooked. Following tephra deposition on Tarso Toussidé, Ehi Sosso developed near the east boundary of the Western TVP. Finally, we see the extrusion of the lavas at Ehi Mousgou appearing to the northwest of Tarso Voon, on top of the most recent Voon tephra deposits.

Phase 6

The final phase of the TVP volcanism was characterized by the formation of Pic Toussidé on the west rim of the pre-Toussidé calderas, as well as several distinct, associated lava flows. The most prominent characteristic of Pic Toussidé is its obvious youth, based on the low visible and IR reflectance and clear definition of the lava flows, as well as the preservation of its cone structure and flanks. The appearance of Timi, in the northern portion of Tarso Toussidé, appears contemporaneous with the formation of Pic Toussidé, and has a fresh, youthful appearance as well, suggesting that weathering has had little time to affect the lava ramparts that make up its flanks. Relatively fresh lava flows and what we interpret as minor pyroclastic deposits on Emi Koussi are apparent in satellite imagery, and we place their development in this later phase as well. Several small, youthful cinder cones appeared on Emi Koussi's flanks, particularly near or within the caldera region.

Most recently, the formation of Trou au Natron took place, which dissected the pre-Toussidé calderas; the Doon Kidimi crater, just east of the pre-Toussidé calderas; and the Era Kohor crater within the caldera system at the summit of Emi Koussi.

Present activity

There have been reports of manifestations of hydrothermal activity associated with the Tibesti massif, such as that at the Soborom Dome (Central TVP), and fumaroles near Emi Koussi at Yi Yerra (Eastern TVP), and at Pic Toussidé (Gèze et al. 1959). Deposition of carbonates at both Trou au Natron and Era Kohor have taken place relatively recently, as has the formation of the volcanic centres on the floor of Trou au Natron. Tarso Tôh, Tarso Toussidé and Emi Koussi are all listed as Holocene in age by the Smithsonian Institution's Global Volcanism Program.

Discussion

Origin and development of the TVP

To account for the origin of the Tibesti massif, Gèze et al. (1959) suggested an upwarping of the basement due to the intrusion of a laccolith. A more contemporary interpretation infers the presence of a mantle plume beneath the cratonic African lithosphere (~130–140 km thick; Ebinger and Sleep 1998). The buoyancy of the plume provided, and sustains, dynamic uplift of the Tibesti massif; early volcanism is likely to have been basaltic (Saunders et al. 1997). Geochemical evidence for the presence of a mantle plume has since been identified by Gourgaud and Vincent (2004). Similar origins have been proposed for other volcanic regions of Africa, including the Cameroon Line, Cameroon (Deruelle et al. 1991); the Hoggar, Algeria (Dautria and Lesquer 1989); and the Darfur Dome, Sudan (Franz et al. 1994).

Waning magma supply from the mantle source would likely result in the compositional evolution of the magma feeding portions of the Tibesti volcanism, ultimately producing late-stage viscous flows and domes (Keddie and Head 1994). At the youthful structure of Emi Koussi, slightly more felsic lavas (Gourgaud and Vincent 2004) sit atop several older, basaltic lapilli tuffs and lava flows. Vincent (1970) originally interpreted the observation of bimodal compositions for lavas within the Tibesti Volcanic Province as the result of two independent magmatic sources. Compositional bimodality such as this could also reflect assimilation of crustal material and magma mixing (Grove 2000). For Emi Koussi, Gourgaud and Vincent (2004) have shown that fractional crystallisation is the main differentiation process for the two mineralogical suites, though for the oversaturated series, crustal contamination probably took place as well. To date, no substantial geochemical or mineralogical data have been reported for any other of the Tibesti's volcanoes.

The volcanoes of the TVP do not show any obvious relationship between age and relative position, as seen, for example, in the case of the Hawaii-Emperor and Cook-Austral volcanic chains. The size, elevations and geographic distribution of the Tibesti volcanoes presumably reflect

the comparatively slow rate of motion of the African Plate with respect to the hot spot reference frame. Burke (1996) describes the African plate as effectively immobile for the past 35 Myr, allowing approximately 40 mantle plumes to penetrate the plate without the creation of any significant hot spot tracks. Likewise, O'Connor et al. (1999) restrict the absolute motion of the African plate to be no more than 20±1 mm/year for at least the past 19 Myr. The prominent linear alignment of Cameroon volcanism (western Africa) is not attributed to hot spot-related tracks above a mobile African plate, but rather as a response to a concentration of extension normal to the Cameroon Line (Burke 2001). The volcanism itself is likely due to pressure relief beneath a line of extended lithosphere, with fairly regular spacing a result of convection (Burke 2001), or is localised by shear zones within the continental lithosphere (Deruelle et al. 1991). Furthermore, Burke (1996) refuted the possibility of plate motion as the mechanism for the observed linearity by postulating an age of <30 Myr for the onset of Cameroon volcanism, just after steady rotation of the African plate had effectively ceased.

Comparisons with other hot spot regions

Pike (1978) makes detailed quantitative comparisons of the gross form of 668 terrestrial and planetary volcanoes, resulting in a statistical analysis using five topographic measurements: height, flank width, and the diameter, depth, and circularity of the summit depression. The morphology of the major structures of Emi Koussi, Tarso Toon, Tarso Voon, Tarso Yega, and Tarso Toussidé fit statistically within what Pike (1978) categorizes as 'alkalic stratocones with summit calderas'. One clear obstacle in otherwise comparing the Tibesti volcanics to other hot spot regions is its relatively unique continental placement. Additionally, the aridity and nature of the Sahara region affords a well-preserved view of the TVP structures from a remote sensing standpoint; compared with some other continental hot spot regions which have been significantly weathered or vegetated (e.g. the Snake River Plain in the western United States). With this in mind, we present straightforward comparisons of the Tibesti volcanic structures to a handful of volcanic hot spot regions on both Earth and Mars. We have chosen a relatively small sample set in an attempt to highlight first-order differences and similarities between more 'conventional' hot spot volcanism and that found within the Tibesti massif. Here, we limit our comparisons to the Hawaiian volcanic chain (Pacific plate), the Galápagos Islands (Nazca plate), the Canary and Cape Verdes archipelagos (African plate), the relatively nearby Jebel Marra in the Darfur region of western Sudan (African Plate), and to large-scale hot spot features on Mars. These regions were singled out for their diversities in location, regional lithospheric thickness, eruption styles, rate of plate motion with respect to an underlying melt source region, and general volcanic geomorphology. Comparisons of the Tibesti Volcanic Province to these locations are summarized in Table 6.

Lithospheric thickness

The Tibesti massif is situated on a stable cratonic region in the centre of the African plate. Ebinger and Sleep (1998) indicated an average lithospheric thickness of ~130–140 km in the proximity of the Tibesti massif. Though similar, it is slightly less at the location of the

Table 6 Comparisons of tectonic and morphological characteristics amongst several terrestrial hot spot regions, the Tharsis Region of Mars, and the Tibesti Volcanic Province, northern Chad

Hot spot region (tectonic setting)	Lithospheric thickness (km)	Volcanic province dimensions (km)	Absolute plate velocity (cm/year)	Avg. caldera diameter (km)	Flank profile	Rift zones/ fissures
Tibesti Volcanic Province (African Plate)	~135	270×220	0.83 WNW	12	~10–30° (steep slopes at summit)	None apparent
Canary Islands (African Plate)	45–95?	570×220	1.05 SW	9	~11–16°	Yes
Cape Verdes (African Plate)	?	300×300	0.95 SW	~7	~4–18°	Yes
Hawaiian Islands (Pacific Plate)	80	720×100	9.53 NW	≤3.5	~3–13° (gentle slopes at summit)	Yes
Galápagos Islands (Nazca Plate)	~15	300×240	3.69 E	5.5	~13–26° (steep slopes at summit)	Yes
Jebel Marra (African Plate)	~110	70×80	0.83 WNW	5	~3–13° (steep slopes at summit)	None apparent
Olympus Mons (Tharsis Region, Mars)	≤500?	550×550	n/a	70	~4°	Likely

2,992-m elevation Jebel Marra volcano in western Sudan (~110 km thickness; Ebinger and Sleep 1998). In comparison, the lithospheric thickness at Hawaii is approximately 80 km (Ribe and Christensen 1999). The lithosphere beneath the Galápagos is relatively young and thin (~15 km; Feighner and Richards 1995). Filmer and McNutt (1989) suggested a thickness of approximately 48 km for the lithosphere beneath the Canary Islands, though Stein and Stein (1992) indicated a much greater thickness of 95±15 km. Data for the Cape Verdes archipelago are sparse, as are data for the volcanic regions of Mars (e.g., Tharsis Bulge). Estimates of the Martian lithospheric thicknesses range from 100 to 500 km (Banerdt et al. 1996) and depend largely on assumed (and as yet unconstrained) values of its lithospheric rigidity and thermal history calculations. The geochemical effects of a thickened crust on rising magma sources (e.g. variations in trace element proportions, silica enrichment due to crustal contamination, etc.) have been investigated in regions such as the central Andes (e.g. Davidson et al. 1991) and Honshu, Japan (e.g. Kersting et al. 1996). The tectonic basis of volcanism throughout these regions is, of course, different from the manifestly intracontinental Tibesti massif, though associations between crustal contamination of rising magma, fractionation of the magma source, and volcanic products could be made with prospective sampling and geochemical analysis of the Tibesti region. The effects on Tibesti volcanism of a thick, cratonic lithosphere above a mantle source are as yet unexplored. In any case, the volcanism in regions most morphologically comparable to the TVP typically lies directly upon oceanic rather than continental crust.

Absolute plate velocity

Due to the slow-moving African plate, the Tibesti Volcanic Province shows no signs of linear tracks of volcanism or age-successive migration of the volcanic centres. The immense sizes (up to ~600 km diameter) of several central Martian volcanoes (e.g. Olympus Mons and the Tharsis Montes) suggest that they, too, reflect at least in part a lack of plate motion relative to a magma source (Zimbelman 2000). Malin (1977) found remarkable similarities in summit caldera and flank morphologies between some of the volcanoes of the Tibesti (Emi Koussi, in particular) and Elysium Mons, Mars. His conclusions indicated that the source of magma for both regions has been essentially stationary with respect to the surface.

Although the Canary Islands do appear to age roughly eastwards (Morgan 1971; Dañobeitia and Canales 2000), historic volcanic activity occurring on several of the islands, including Lanzarote, Gran Canaria, and Tenerife (Simkin and Siebert 1994), complicate the picture of a simple age progression of the archipelago (e.g. Hoernle and Schmincke 1993). Likewise, the Cape Verdes Islands show a broad age progression from east (older) to west (younger) (Phipps Morgan et al. 1995). Nine of the western Galápagos volcanoes have erupted within the past 200 years (McClelland et al. 1989; Global Volcanism Network 1991a,b; Simkin and Siebert 1994), with no clear age progression. Though the rate of motion of the Nazca Plate above the Galápagos magma source (51 mm/year; Gripp and Gordon 1990) is significantly higher than that of the African plate, the focusing of magma supply below the Galápagos appears not simply to be controlled by plate motion (Rowland et al. 1994). The linear and age-related Hawaiian hot spot trend differs from all of these hot spots due to the high velocity of the Pacific plate above the established mantle plume.

Flank profile

In terms of gross morphology, the base and mid-flank regions of Tibesti volcanoes share similar slopes (~4–12°) to those in Hawaii (3–13°; Mark and Moore 1987), as well as to many in the Galápagos. The major Hawaiian volcanoes tend to retain their gentle slopes at their summit regions, whereas several Tibesti volcanoes (Emi Koussi, Pic Toussidé, Tarsos Toon and Yega, in particular) exhibit steepened slopes as their summits are approached. The summit regions of both the Tibesti and Galápagos volcanoes are similarly steep, though in the case of the Galápagos, slopes are suggested to be due primarily to prolonged wave erosion of the outer flanks, modifying the gradients at lower levels (Rowland et al. 1994). The topographic profiles of shield volcanoes within the Galápagos archipelago range widely from values similar to Hawaiian volcanoes, up to 20–26° in some areas (Nordlie 1973). The summit and basal flanks of Jebel Marra, in Sudan, have morphological similarities to those of Emi Koussi and to those of the Galápagos, in particular, with gradients upwards of 13° at the central crater rim and a relatively abrupt levelling off of approximately 3° towards the mid-flank and base regions.

Rift zones/ fissures

Based on overt resemblances to the Galápagos volcanoes and Jebel Marra in gross morphology, we suggest that there may be similar development of the Tibesti Volcanic Province, the volcanism in the Galápagos, and western Sudan, despite differences in setting and scale.

The volcanoes of the Galápagos Islands are principally basaltic shields with relatively large summit calderas (~5 km diameter). In contrast to what we infer about the nature of the Tibesti Volcanic Province, most eruptions of Galápagos volcanoes are from either radial or circumferen-

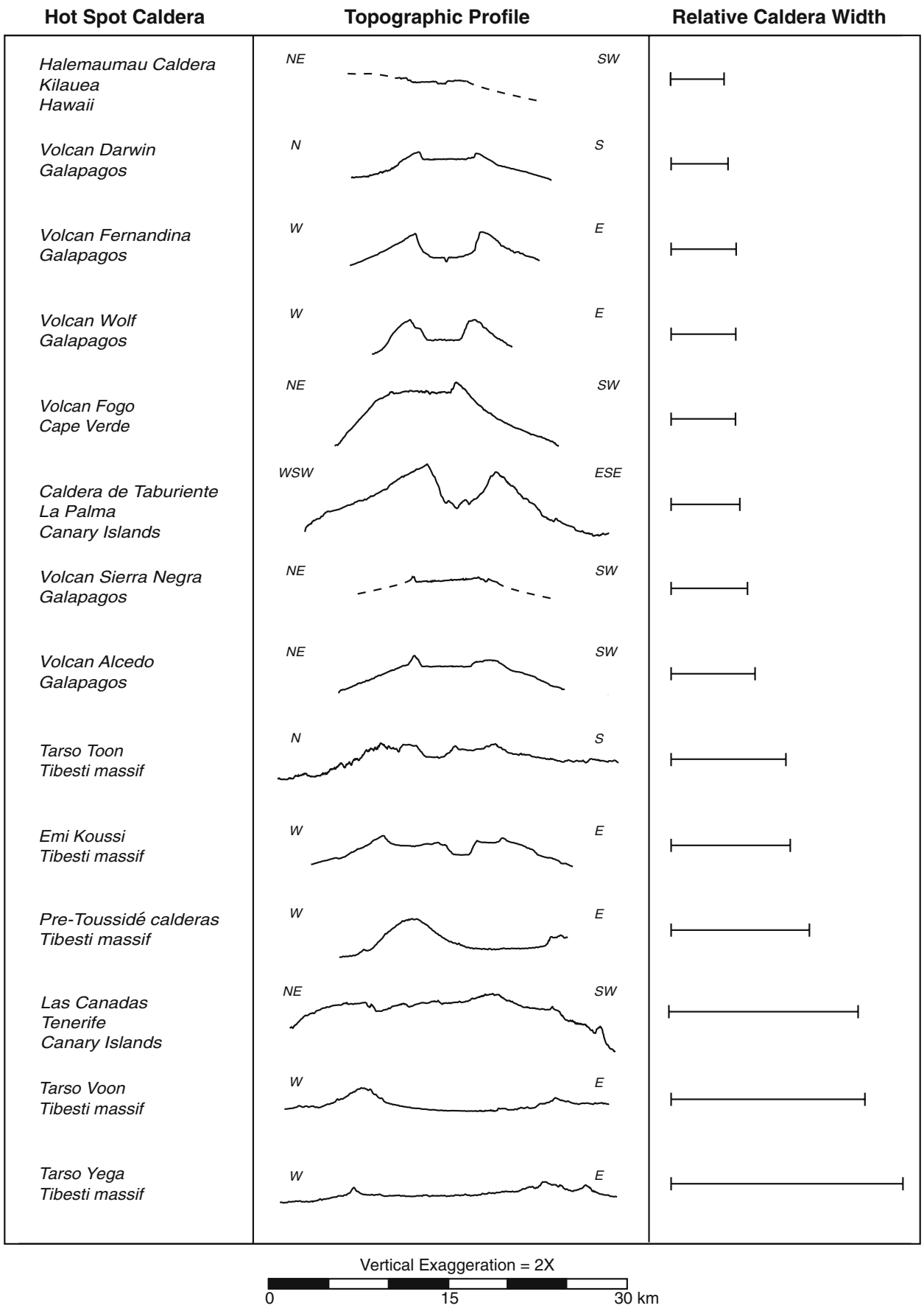
Hot Spot Caldera
Topographic Profile
Relative Caldera Width
Halemaumau Caldera
Kilauea
Hawaii
NE
SW
Volcan Darwin
Galapagos
N
S
Volcan Fernandina
Galapagos
W
E
Volcan Wolf
Galapagos
W
E
Volcan Fogo
Cape Verde
NE
SW
Caldera de Taburiente
La Palma
Canary Islands
WSW
ESE
Volcan Sierra Negra
Galapagos
NE
SW
Volcan Alcedo
Galapagos
NE
SW
Tarso Toon
Tibesti massif
N
S
Emi Koussi
Tibesti massif
W
E
Pre-Toussidé calderas
Tibesti massif
W
E
Las Canadas
Tenerife
Canary Islands
NE
SW
Tarso Voon
Tibesti massif
W
E
Tarso Yega
Tibesti massif
W
E
Vertical Exaggeration = 2X
0
15
30 km

tial eruptive fissures. These fissures are the surface expression of dikes that have reached the surface (Chadwick and Howard 1991). In the case of the Hawaiian Islands, long, narrow rift zones have developed as a result of dike intrusion (e.g. Swanson et al. 1976; Cervelli et al. 2002). Effects of gravity on both the volcanic edifice and magmatic system have also resulted in the development of a prominent rift system in the Canary Islands (Ablay and Marti 2000), which possess the highest proportion of fissure vent volcanoes as primary features (Simkin and Siebert 1994). The existence of eruptive fissures or rift zones in association with the Tibesti massif has not been previously reported, and is not apparent in satellite imagery we have examined.

Caldera formation and morphology

Variations in subsidence geometries with respect to widespread caldera collapse events are discussed by Lipman (1997) and Walker (1984); the collapse style of a caldera can typically be inferred from the size of the existing caldera structure. Comparisons amongst several hot spot-related calderas (Fig. 5) indicate that the areas and dimensions of Tibesti calderas fall in the moderate- to high-end of the spectrum (~12 km in diameter). Indeed, the above-average diameters of Tibesti calderas may correlate with the size of underlying magma reservoirs (cf. Lipman 1997). Based on the scale and characteristics of the Tibesti calderas, we postulate that the underlying mechanism for caldera collapse in the TVP has largely involved plate (piston) subsidence of a relatively coherent floor. Subordinate downsag could be a possible explanation for the slightly depressed floors of Tarso Voon, Tarso Yega, and the pre-Toussidé calderas. Clear evidence of piecemeal or multicyclic subsidence (e.g. stepped block faulting of the caldera floor, arcuate growth faults) has not been observed in most of the Tibesti volcanoes, though the stepped summit of Emi Koussi could potentially suggest multi-stage development. The presence of relatively well-defined rims and planar floors within the majority of Tibesti calderas exclude the likelihood that asymmetric subsidence has taken place. Future fieldwork is needed to determine the style of caldera formation for each of these centres.

Calderas associated with Hawaiian volcanoes have developed by the loading of dense cumulates beneath the volcanic edifice, promoted by thermal weakening of the volcanic pile (e.g. Peterson and Moore 1987). Evidence for this type of mechanism includes positive gravity anomalies over the calderas, a stepped, funnel-shaped deformation profile, inward-dipping flows, and a large discrepancy in erupted volume versus subsidence volume (Walker 1984, 1988). Morphological characteristics such as these are not evident in the satellite imagery we have analysed of the TVP structures, though that does not completely preclude their presence. Data required to provide estimates of erupted and subsidence volumes of the TVP volcanoes have not yet been produced. Additionally, gravimetric data are not yet available at sufficient resolution for the Tibesti region to distinguish small-scale anomalies for better comparison.

The Las Cañadas nested collapse caldera (Tenerife, Canary Islands) is more comparable in scale to many calderas within the Tibesti Volcanic Province (see Fig. 5). Its present morphology reflects the successive migration and collapse of shallow magmatic chambers (Marti and Gudmundsson 2000), and has gradually enlarged over >2.3 Myr to a 25 km diameter due to successive flank failures (Cantagrel et al. 1999). Interestingly, evidence of significant flank failures is not apparent in satellite imagery of the TVP, however, and none has been reported previously. Several volcanoes within the Galápagos display near-vertical ring faults circumscribing their summits (e.g. Simkin and Howard 1970; Reynolds et al. 1995). A few related features (e.g. small volcanic extrusions, maars, cinder cones) can be seen in proximity to some Tibesti volcanoes (Emi Koussi and Tarso Voon, in particular) that may provide evidence for caldera-related ring faults, though no ring faulting is readily apparent in satellite imagery.

Based on these first-order comparisons, we suggest that the major Tibesti calderas appear to have formed by events similar to those found in the Galápagos (cf. Simkin and Howard 1970). The nearby Jebel Marra main volcanic centre shows similarities to Emi Koussi in satellite imagery as well, and the tectonic setting is, of course, similar.

◀ **Fig. 5** Comparison amongst several hot spot caldera system dimensions, including both oceanic and continental regimes. Calderas associated with the Tibesti volcanoes are significantly larger than most other examples seen here. Caldera profiles for all structures were created using ASTER-based digital elevation models. Vertical exaggeration=2×

Conclusions

Based on detailed analyses of satellite imagery, mostly from the high-resolution ASTER instrument, we have updated the only previous synoptic study of the volcanology of the Tibesti massif by Gèze et al. (1959). The relative inaccessibility of the Tibesti massif for most researchers establishes a prime example of the utility of remote sensing as an effective and efficient tool for volcanological investigation under such circumstances.

We propose that the TVP lacks any clear spatial progression of volcanic centres, though volcanism seems to have initiated in the Central TVP (e.g. Tarsos Voon and Toon). Volcanism subsequently migrated to the Eastern and

Western TVP regions, developing substantial lava plateaux and additional volcanic features (including both Emi Koussi and Pic Toussidé). Geochronological investigations will be needed to further establish the details of TVP development, though estimates place the Tibesti volcanism to Late Miocene and younger (Gourgaud and Vincent 2004).

Comparisons with other hot spot volcanoes (e.g. the Hawaiian hot spot track, the Galápagos Islands, the Canary and Cape Verdes archipelagos, Jebel Marra, and Martian volcanoes) point to distinctions of the TVP, including the thickness and slow velocity of the lithosphere beneath the Tibesti region, its intracontinental tectonic setting, and its extent and diversity of volcanic features. The TVP does not present a linear hot spot track as seen, for example, in the case of the Hawaii-Emperor volcanic chain. The large scale of TVP calderas and the inferred plate subsidence and downsag as their primary collapse mechanisms point to further differences from other hot spot volcanoes. Future studies of the TVP are clearly warranted to further our understanding of the causes of these distinctions, including more detailed radiometric dating and reconnaissance-scale petrological and geochemical investigations. Relative volumes of the erupted vs. subsided material for each of the TVP volcanoes (and therefore the whole of the TVP) have not as-yet been constrained using remote sensing techniques. The lack of data concerning the elevation of the sedimentary basement, make volumetric estimates of the TVP volcanics difficult. Further, values could vary by orders of magnitude depending upon speculated thicknesses of erupted lava and/or tephra deposits. Again, future field investigations will be needed to provide robust estimates of volumes of products. A systematic, reconnaissance-scale field survey would greatly advance our understanding of the Tibesti Volcanic Province, and continental hot spot volcanism more generally, and we hope that this contribution stimulates further research of this fascinating region.

Acknowledgements We thank the ASTER team, and especially Elsa Abbott (NASA-JPL), for help and advice with the ASTER imagery and processing, and NASA's EOSDIS for data and support. We are also grateful to Rob Jones and Kevin Lawless at RSI, UK, for their help in acquiring and servicing ENVI software and related modules. We are deeply grateful to Shan de Silva and David Crown for their invaluable comments and advice for revision of the original manuscript.

References

Ablay GJ, Marti J (2000) Stratigraphy, structure, and volcanic evolution of the Pico Teide–Pico Viejo formation, Tenerife, Canary Islands. J Geophys Res 103:175–208

Abrams M, Hook SJ (1995) Simulated Aster data for geologic studies. IEEE Trans Geosci Remote Sens 33:692–699

Banerdt B, Chicarro AF, Coradini M, Federico C, Greeley R, Hechler M, Knudsen JM, Leovy C, Lognonné Ph, Lowry L, McCleese D, McKay C, Pellinen R, Phillips R, Scoon GEN, Spohn T, Squyres S, Taylor F, Wänke H (1996) INTERMARSNET Phase-A Study Report. ESA Publication D/SCI(96)2

Burke K (1996) The African plate. S Afr J Geol 99:339–410

Burke K (2001) Origin of the Cameroon line of volcano-capped swells. J Geol 109:349–362

Cahen L, Snelling NJ, Delhal J, Vail JR (1984) The geochronology and evolution of Africa. Clarendon, Oxford, p 512

Cantagrel JM, Arnaud NO, Ancochea E, Fuster JM, Huertas MJ (1999) Repeated debris avalanches on Tenerife and genesis of Las Cañadas caldera wall (Canary Islands). Geology 27:739–742

Cervelli P, Segall P, Amelung F, Garbeil H, Meertens C, Owen S, Miklius A, Lisowski M (2002) The 12 September 1999 Upper East Rift Zone dike intrusion at Kilauea Volcano, Hawaii. J Geophys Res 107:2150. DOI 10.1029/2001JB000602

Chadwick WW Jr, Howard KA (1991) The pattern of circumferential and radial eruptive fissures on the volcanoes of Fernandina and Isabela islands, Galápagos. Bull Volcanol 53:259–275

Cohen R (1994) "Chad wins world court decision in territorial dispute with Libya." The New York Times, February 4, p A6

Crough ST (1978) Thermal origin of mid-plate hotspot swells. Geophys J R Astron Soc 55:451–469

Dañobeitia JJ, Canales JP (2000) Magmatic underplating in the Canary Archipelago. J Volcanol Geotherm Res 103:27–41

Dautria JM, Lesquer A (1989) An example of the relationship between rift and dome: recent geodynamic evolution of the Hoggar swell and of its nearby regions (Central Sahara, Southern Algeria and Eastern Niger). Tectonophysics 163:45–61

Davidson JP, Harmon RS, Worner G (1991) The source of central Andean magmas: some considerations. In: Harmon RS, Rapella CW (eds) Andean magmatism and its tectonic setting. Geol Soc Am Spec Paper 265:233–244

Davies AG, Keszthelyi LP, Williams DA, Phillips CB, McEwen AS, Lopes RMC, Smythe WD, Kamp LW, Soderblom LA, Carlson RW (2001) Thermal signature, eruption style, and eruption evolution at Pele and Pillan on Io. J Geophys Res 106:33, 079–33, 103

Deruelle B, Moreau C, Nkoumbou C, Kambou R, Lissom J, Njonfang E, Ghogomu RT, Nono A (1991) The Cameroon line: a review. In: Kampunzu AB, Lubala RT (eds) Magmatism in extensional structural settings, the Phanerozoic African Plate. Springer, Berlin Heidelberg New York, pp 274–327

de Silva SL, Francis P (1990) Potentially active volcanoes of Peru—observations using Landsat Thematic Mapper and Space Shuttle imagery. Bull Volcanol 52:286–301

Dziewonski AM, Chou TA, Woodhouse JH (1981) Determination of earthquake source parameters from waveform data for studies of global and regional seismicity. J Geophys Res 86:2825–2852

Earth Sciences and Image Analysis, NASA-Johnson Space Center (27 Jun. 2003) "The Gateway to Astronaut Photography of Earth." <http://eol.jsc.nasa.gov/Info/use.htm> (2 Nov. 2003)

Ebinger CJ, Sleep NH (1998) Cenozoic magmatism throughout East Africa resulting from impact of a single plume. Nature 395:1788–1791

El Makhrouf AA (1988) Tectonic interpretation of Jabal Eghei area and its regional application to Tibesti orogenic belt, south central Libya (S.P.L.A.J.). J Afr Earth Sci 7:945–967

Feighner MA, Richards MA (1995) Lithospheric structure and compensation mechanisms of the Galapagos archipelago. J Geophys Res 99:6711–6729

Filmer PE, McNutt MK (1989) Geoid anomalies over the Canary Islands Group. Mar Geophys Res 11:77–87
Franz G, Pudlo D, Urlacher G, Haussmann U, Boven A, Wemmer K (1994) The Darfur dome, western Sudan: the product of a subcontinental mantle plume. Geol Rundsch 83:614–623
Furon R (1963) Geology of Africa. Oliver & Boyd, Edinburgh (trans 1963, orig French 1960), pp 1–377
Gèze B, Hudeley H, Vincent P, Wacrenier P (1959) The volcanoes of the Tibesti (Sahara of Chad) (in French). Bull Volcanologique 22:135–188
Ghuma MA, Rogers JJW (1978) Geology, geochemistry, and tectonic setting of the Ben Ghnema batholith, Tibesti massif, southern Libya. Geol Soc Am Bull 89:1351–1358
Global Volcanism Network (1991a) Report for August 1991, p 15
Global Volcanism Network (1991b) Report for September 1991, p 4
Goodell PC (1992) Uranium potential of the Tibesti and Hoggar massifs, north–central Africa. Geol Libya 7:2627–2637
Gourgaud A, Vincent PM (2004) Petrology of two continental alkaline intraplate series at Emi Koussi volcano, Tibesti, Chad. J Volcanol Geotherm Res 129:261–290
Gripp AE, Gordon RG (1990) Current plate velocities relative to the hotspots incorporating the NUVEL-1 global plate motion model. Geophys Res Lett 17:1109–1112
Grove A (1960) Geomorphology of the Tibesti region with special reference to western Tibesti. Geograph J 126:18–31
Grove TI (2000) Origin of magmas. In: Sigurdsson H (ed) Encyclopedia of volcanoes. Academic, San Diego, pp 133–147
Guiraud R, Doumnang Mbaigane J-C, Carretier S, Dominguez (2000) Evidence for a 6000 km length NW–SE striking lineament in northern African: the Tibesti Lineament. J Geol Soc (Lond) 157:897–900
Hagedorn H, Jakel D (1969) Bemerkungen zur quartaren Entwicklung des Reliefim Tibesti-Gebirge (Tchad). Bulletin de Liaison de l'Association senegalaise pour l'Etude duQuaternaire africain 23:25–42
Hoernle K, Schmincke HU (1993) The role of partial melting in the 15-Ma geochemical evolution of Gran Canaria: a blob model for the Canary hotspot. J Petrol 34:599–626
Hubbard BE, Crowley JK, Zimbelman DR (2003) Comparative alteration mineral mapping using visible to shortwave infrared (0.4–2.4 μm) Hyperion, ALI, and ASTER imagery. IEEE Trans Geosci Rem Sens 41:1401–1410
International Campaign to Ban Landmines (2001) Landmine Monitor Report 2001: toward a mine-free world. Human Rights Watch, New York, p 1175
Kahle A, Abrams M, Abbott E, Mouginis-Mark P, Realmuto V (1995) Remote sensing of Mauna Loa. In: Rhodes JM, Lockwood JP (eds) Mauna Loa revealed: structure, composition, history, and hazards. Geophys Monog 92, AGU, p 348
Kahle AB, Goetz FH (1983) Mineralogic information from a new airborne thermal infrared multispectral scanner. Science 222:24–27
Kahle AB, Palluconi FD, Hook SJ, Realmuto VJ, Bothwell G (1991) The advanced spaceborne thermal emission and reflectance radiometer (ASTER). Intl J Imag Sys Technol 3:144–156
Keddie ST, Head JW (1994) Height and altitude distribution of large volcanoes on Venus. Planet Space Sci 42:456–462
Kersting AB, Arculus RJ, Gust DA (1996) Lithospheric contributions to arc magmatism: isotope variations along-strike in volcanoes of Honshu, Japan. Science 272:1464–1468
Lipman PW (1997) Subsidence of ash-flow calderas: relation to caldera size and chamber geometry. Bull Volcanol 59:198–218
Malin M (1977) Comparison of volcanic features of Elysium (Mars) and Tibesti (Earth). GSA Bull 88:908–919
Mark RK, Moore JG (1987) Slopes of the Hawaiian Ridge. US Geol Surv Prof Pap 1350:101–107
Marti J, Gudmundsson A (2000) The Las Cañadas caldera (Tenerife, Canary Islands): an overlapping collapse caldera generated by magma-chamber migration. J Volcanol Geotherm Res 103:161–173
McClelland L, Simkin T, Summers M, Nielson E, Stein TC (1989) Global volcanism 1975–1985. Prentice Hall, Englewood Cliffs, p 655
Morgan WJ (1971) Convection plumes in the lower mantle. Nature 230:42–44
Morgan WJ (1972) Deep mantle convection plume and plate motions. Am Assoc Petrol Geol Bull 56:203–312
Mouginis-Mark PJ, Robinson MS (1992) Evolution of the Olympus Mons caldera, Mars. Bull Volcanol 54:347–360
Nordlie BE (1973) Morphology and structure of the western Galapagos volcanoes and a model for their origin. Geol Soc Am Bull 84:2931–2956
O'Connor JM, Stoffers P, van den Bogaard P, McWilliams M (1999) First seamount age evidence for significantly lower African plate motion since 19 to 30 Ma. Earth Planet Sci Lett 171:575–589
Okada K, Ishii M (1993) Mineral and lithological mapping using thermal infrared remotely sensed data from ASTER simulator. Geoscience and Remote Sensing Symposium, 1993. IGARSS '93. 'Better Understanding of Earth Environment', International 1:126-128. DOI 10.1109/IGARSS.1993.322501
Oppenheimer C (1998) Volcanological applications of meteorological satellites. Int J Rem Sens 19:2829–2864
Perfit MR, Davidson JP (2000) Plate tectonics and volcanism. In: Sigurdsson H (ed) Encyclopedia of volcanoes. Academic, San Diego, pp 89–113
Peterson DW, Moore RB (1987) Geologic history and evolution of geologic concepts, island of Hawaii. US Geol Surv Prof Pap 1350:149–189
Phipps Morgan J, Morgan WJ, and Price E (1995) Hotspot melting generates both hotspot volcanism and a hotspot swell? J Geophys Res 100:8045–8062
Pieri D, Abrams M (2004) ASTER watches the world's volcanoes: a new paradigm for volcanological observations from orbit. In: Ramsey M, Flynn L, Wright R (eds) (2004) Volcanic observations from space: new results from the EOS satellite instruments. J Volcanol Geotherm Res 135:13–28
Pike RJ (1978) Volcanoes on the inner planets: some preliminary comparisons of gross topography. Proc Lunar Planet Sci Conf 9:3239–3273
Ramsey M, Flynn L, Wright R (eds) (2004) Volcanic Observations from Space: New Results from the EOS satellite instruments. J Volcanol Geotherm Res 135:1–219
Reynolds RW, Geist D, Kurz MD (1995) Physical volcanology and structural development of Sierra Negra volcano, Isabela Island, Galapagos archipelago. Bull Geol Soc Am 107:1398–1410
Ribe NM, Christensen UR (1999) The dynamical origin of Hawaiian volcanism. Earth Planet Sci Lett 171:517–531
Rowland SK, Munro DC, Perez-Oviedo V (1994) Volcan Ecuador, Galapagos Islands: erosion as a possible mechanism for the generation of steep-sided basaltic volcanoes. Bull Volcanol 56:271–283
Saunders AD, Fitton JG, Kerr AC, Norry MJ, Kent RW (1997) The North Atlantic igneous province. In: Mahoney JJ, Coffin MF (eds) Large Igneous Provinces. Geophys Monogr, AGU, pp 45–94
Simkin T, Howard KA (1970) Caldera collapse in the Galapagos Islands. Science 169:429–437
Simkin T, Siebert L (1994) Volcanoes of the world, 2nd edn. Geoscience, Tucson, pp 349
Smith RB, Braile LW (1994) The Yellowstone hotspot. J Volcanol Geotherm Res 61:121–187

Stein CA, Stein S (1992) A model for the global variation in oceanic depth and heat-flow with lithospheric age. Nature 359:123–129

Survey Action Center (2002) Landmine Impact Survey: Republic of Chad. Vietnam Veterans of America, Washington DC, p 188

Swanson DA, Duffield WA, Fiske RS (1976) Displacement of the south flank of Kilauea volcano: the result of forceful intrusion of magma into the rift zones. U S Geol Surv Prof Paper 963:39

Tilho J (1920) The exploration of Tibesti, Erdi, Borkou, and Ennedi in 1912–1917. Geograph J 56:81–99, 161–183, 241–263

Vachette M (1964) Radiometric ages of crystalline formations of equatorial Africa (Gabon, Central African Republic, Chad, Middle Congo) (in French). Ann Fac Sci Univ Clermont 25:1–31

Vincent PM (1970) The evolution of the Tibesti Volcanic Province, eastern Sahara. In: Clifford TN, Gass IG (eds) African Magmatism and Tectonics. Oliver & Boyd, Edinburgh, pp 461

Walker GPL (1984) Downsag calderas, ring faults, caldera sizes, and incremental caldera growth. J Geothermal Res 89:8407–8416

Walker GPL (1988) Three Hawaiian calderas: an origin through loading by shallow intrusions? J Geophys Res 93:14773–147784

White RS, McKenzie DP (1995) Mantle plumes and flood basalts. J Geophys Res 100:17543–17585

Wiart P, Oppenheimer C (2005), Large magnitude silicic volcanism in north Afar: The Nabro Volcanic Range and Ma'alalta volcano. Bull Volcanol 67:99-115. DOI 10.1007/s00445-004-0362-x

Yamaguchi Y, Kahle AB, Tsu H, Kawakami T, Moshe P (1998) Overview of advanced spaceborne thermal emission and reflection radiometer (ASTER). IEEE Trans Geosci Rem Sens 36:1062–1071

Zhao D (2001) Seismic structure and origin of hotspots and mantle plumes. Earth Planet Sci Lett 192:251–265. DOI 10.1016/s0012-821X(01)00465-4

Zhao D (2004) Global tomographic images of mantle plumes and subducting slabs: insight into deep Earth dynamics. Phys Earth Planet Inter 143:3–34. DOI 10.1016/j.pepi.2003.07.032

Zimbelman JR (2000) Volcanism on Mars. In: Sigurdsson H (ed) Encyclopedia of volcanoes. Academic, San Diego, pp 771–783